Ring-Shaped Discharge Structures in a Closed Cycle MHD Disk Generator

Hiroshi Fukuda* and Shigeharu Kabashima†
Tokyo Institute of Technology, Yokohama, Japan

Numerical simulations are carried out to study plasma properties in a nonequilibrium disk-type MHD generator. The analysis is based on a two-dimensional time-dependent MHD equation, and is performed in the *r-z* plane. From the *r-z* analysis, we can get the current distributions in the boundary layer, electrode regions, as well as the channel main flow region. The two-state nature of plasma, i.e., the formation of streamers and their dynamical behavior in the channel is confirmed. The dependence of the streamer properties on the magnetic field strength and load resistance is examined. The calculations suggest the existence of an eddy current in the boundary layer for the high-loading parameter. Some enhanced eddy currents in the nozzle region and the intensive eddy current at the upper-stream edge of the cathode are obtained for some plasma parameters.

Introduction

RECENT experimental results of some nonequilibrium disk-type MHD generators indicated the following facts.

1) It was frequently observed that the strong discharge structures (streamers) generated in the upstream part of the channel moved downstream repeatedly in the case of the low loading parameter.[1,2]

2) A wide "inlet relaxation region" was observed in this situation.[1-3]

3) The existence of some Joule heating in the nozzle was also predicted.[3]

The aim of this paper is to give some explanations for these facts from the viewpoint of numerical simulation.

Most of the analyses regarding nonequilibrium disk-type MHD generators, have been carried out in the *r-θ* plane, because nonuniformity due to the ionization instability essentially grows in this plane.[4-6] No analysis has been made regarding the current distributions in the boundary layer and in the electrode region, although these effects evidently cause the nonuniformity in the *r-z* plane. For example, the possibility that eddy current exists in the boundary layer is expected when the Hall field becomes high.

In this work, the time-dependent analysis has been performed for a nonequilibrium disk-type MHD generator in the *r-z* plane. The region in which MHD equations are being solved include the nozzle region which is used as the anode, and cathode region. Using this scheme, we will be able to discuss the problems mentioned earlier and, most importantly, we will be able to get reliable information about inlet relaxation without artificial assumptions for the inlet of the channel.

Basic Equations

The development of the dynamical equations for the simulations are based on the two-temperature model. In this paper, we confine our attention to the behaviors of the plasma; therefore, we assume that the gasdynamic variables remain constant in space and time. The conventional MHD approximations of charge neutrality and low magnetic Reynolds number are also adopted. As a result, equations of nonequilibrium plasma can be given as:

Continuity equation:

$$\frac{\partial n_s^+}{\partial t}+\nabla\cdot(n_s^+\cdot u)=\dot{n}_s^+,\quad \frac{\partial n_a^+}{\partial t}+\nabla\cdot(n_a^+\cdot u)=\dot{n}_a^+ \tag{1}$$

Generalized Ohm's law:

$$J+\frac{\beta}{B}J\times B=\sigma\left(E+u\times B+\frac{\nabla p_e}{en_e}\right) \tag{2}$$

Energy equation:

$$\frac{\partial U_e}{\partial t}+\nabla\cdot(U_e u_e)=\frac{J^2}{\sigma}-A-Q_r-p_e\nabla\cdot u_e \tag{3}$$

Maxwell equations:

$$\mathrm{rot}E=0 \tag{4a}$$

$$\mathrm{div}J=0 \tag{4b}$$

where

$$n_j=k_j n_e n_j-k_r n_e^2 n_j^+ \qquad (j=s,\ a)$$

$$p_e=n_e kT_e$$

$$U_e=\frac{3}{2}n_e kT_e+n_s^+\epsilon_s+n_a^+\epsilon_a$$

$$A=\frac{3}{2}\delta n_e m_e k(T_e-T_g)\sum_j\frac{\nu_j}{m_j} \qquad (j=s,a,i)$$

Q_r represents the radiation loss of plasma,[16] and subscripts *s*, *a*, and *i* denote seed atoms, noble gas atoms and heavy ions, respectively. All notations are conventional ones and are used in Refs. 7-11.

The configuration of the disk-type MHD generator considered here is shown in Fig. 1, where calculations are carried out in the hatched region. A cylindrical coordinate system is adopted and the directions of flow and magnetic fields are set same as shown in this figure. The conventional boundary conditions for electromagnetic fields are taken on the insulator and electrodes, and other boundary conditions are taken as

Received Jan. 22, 1986; revision received May 27, 1986.

*Graduate Student, Department of Energy Sciences; currently with Central Research Laboratory of Hitachi Ltd., Kokubunzi, Tokyo, Japan.

†Associate Professor, Department of Energy Sciences.

follows: $J_z=0$ on the plane of $z=0$, and $J_r=0$ at the inlet of the nozzle and the outlet of the cathode region. The tangential component of the heavy particle velocity is assumed to be zero, and all the quantities are assumed to be constant in the θ-direction. An initial electron temperature is given by the Gaussian distribution whose mean value and standard deviation is 3000 and 30 K, respectively. An initial electron density is assumed to be the Saha equilibrium value corresponding to that electron temperature. The working gas considered in this analysis is a potassium-seeded argon. The conditions of magnetic field strength, seed fraction, etc. used in the following calculations are selected to fit for the power generation conditions and listed in Table 1.

By substituting Eq. (2) into Eq. (4a) and expressing it in the cylindrical coordinate system, we obtain[5,10,11]

$$\frac{\partial}{\partial r}\left(\frac{1}{\sigma r}\frac{\partial \psi}{\partial r}\right)+\frac{\partial}{\partial z}\left(\frac{1+\beta^2}{\sigma r}\frac{\partial \psi}{\partial z}\right) = -\frac{\partial}{\partial r}\left(\frac{1}{en_e}\frac{\partial p_e}{\partial z}\right)+\frac{\partial}{\partial z}\left(\beta uB+\frac{1}{en_e}\frac{\partial p_e}{\partial r}\right) \tag{5}$$

using a current stream function defined as

$$J_r=\frac{1}{r}\frac{\partial \psi}{\partial z},\quad J_z=-\frac{1}{r}\frac{\partial \psi}{\partial r} \tag{6}$$

If the distribution of plasma properties is given, Eq. (5) can be solved by means of the finite element method. Changes of electron temperature T_e and electron number density n_e are obtained from Eqs. (3) and (1), respectively.

Formation of a Streamer and Its Dynamical Behavior

In this section we concentrate our interest on the ionization instability of the plasma, i.e., the formation of a streamer and its dynamical behavior. So, we discuss the plasma behavior in a constant cross-section generator, whose dimension is shown in Fig. 1.

Result of Numerical Simulation

Figure 2 shows a typical example of the evolutions of the distributions of T_e, n_e, and electrical potential ϕ along the r-direction. It is seen that in this load condition the Joule heating in the generator is not enough to ionize all the seed atoms, so that plasma grows to form two states. The first in which the values of T_e and n_e are rather large, consists of the fully ionized seed plasma, and we call this region "state-1." The second, in which the values of T_e and n_e are rather small due to only slightly ionized seed, is called "state-2." In each state, T_e and n_e are almost uniform. As in the case of Faraday-type generators, state-1 can be known as "streamer." The electric field in the region of state-2 directs opposite to that of state-1, so the broad region of state-2 reduces the generator performance. The two-state nature of plasma corresponds to the local plasma analysis by Mesland.[11] Some two-dimensional analyses on nonequilibrium MHD generators also show this tendency of plasma behavior.[4-6,17]

Another interesting fact demonstrated by these figures is that the streamer initially flows downstream with the fluid velocity, keeping its width constant. When the streamer reaches the end of the channel, it halts there. As a result, a broad region of state-2 appears in the inlet region of the channel, which is usually called the inlet relaxation region. In this case, the streamer halts in the downstream of the generator, but in the case of a generator, which has more loss of electron energy, the flow of the streamer repeats. This will be discussed later. This behavior relates to the growth condition of the plasma; however, actual criterion could not be achieved.

In Fig. 3 we show the dependence of plasma properties on the magnetic field strength B and the external load resistance R_l. Figure 3a and 3b show the evolutions of the distribution of n_e along the r-direction when B and R_l are increased, respectively, as compared to the condition for Fig. 2. These figures show that the main factor which governs the width of the

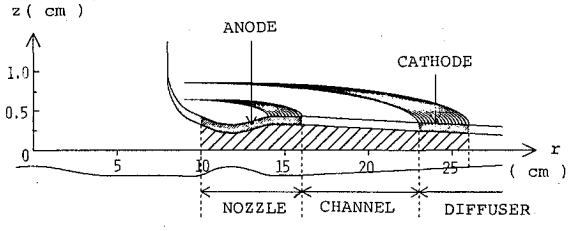

Fig. 1 Configuration of disk MHD generator and coordinate system. Inlet height of the generator is 8.4 mm.

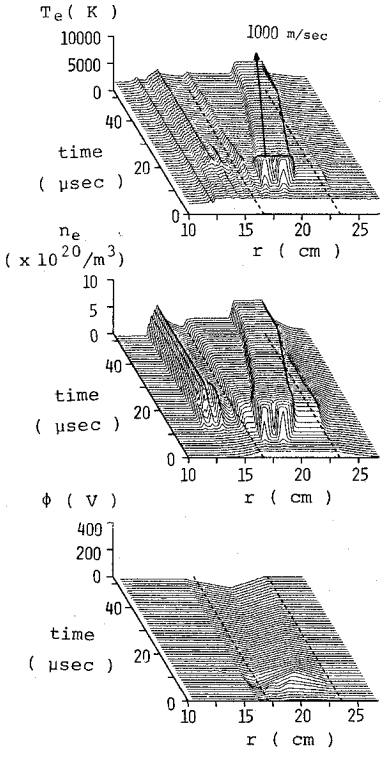

Fig. 2 Evolutions of the distribution of a) T_e, b) n_e, c) potential along the r-direction. $B=5T$; $R_l=0.1\Omega$.

Table 1 Conditions used in the numerical simulations

Section	Magnetic field strength, T	Load resistance, Ω	Seed fraction	Stagnation pressure, atm	Stagnation temperature, K	Channel Mach number
3	3,5,7	0.02~8	5×10^{-5}	10	2000	1.7
4	7	4	5×10^{-5}	10	2000	1.7
5	3,5,7	4,6	5×10^{-5}	10	2000	1.7

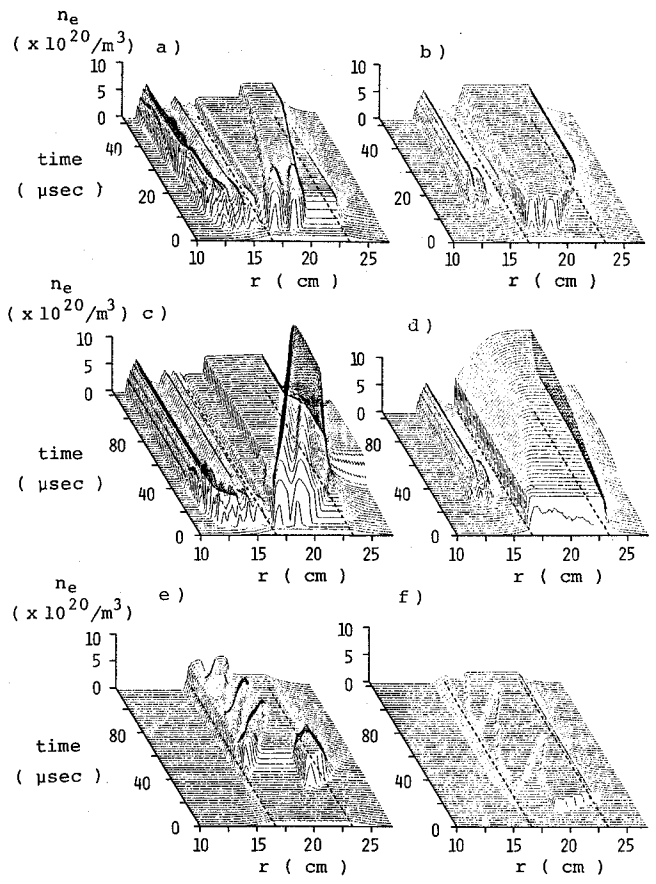

Fig. 3 Evolutions of the distribution of n_e in the r-direction for various parameters. a) $B=7T$, $R_l=0.1\Omega$; b) $B=5T$, $R_l=1.0\Omega$; c) $B=7T$, $R_l=1.0\Omega$; d) $B=5T$, $R_l=8.0\Omega$; e) $B=3T$, $R_l=0.02\Omega$; f) $\delta=20$, $B=5T$, $R_l=1.0\Omega$.

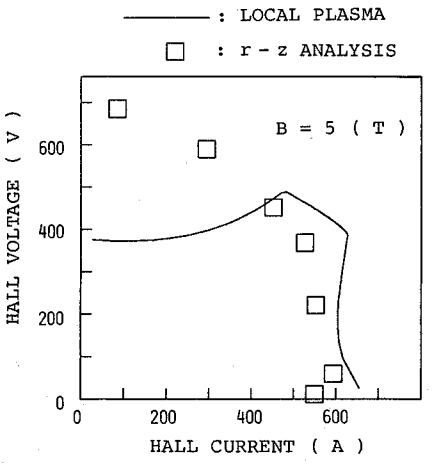

Fig. 4 V-I characteristics of the generator, $B=5T$. Solid curve shows the results of the steady-state analysis of the local plasma using σ_{eff} and β_{eff}, and the squares show results of r-z analysis.

streamer is R_l in these working gas conditions. In Fig. 3b, the fully ionized seed plasma is found in almost the whole channel. Figures 3c and 3d show the results when B and R_l are increased, respectively, as compared to Fig. 3b. In Fig. 3d, the value of T_e in state-1 is high enough to ionize noble gas atoms, and n_e increases rapidly because of the ionization of the noble gas. However, in Fig. 3c, the region of the noble gas ionization builds up initially because of the smallness of initial n_e, and the fully ionized seed plasma appears in the whole channel after the growth of the initial noble gas ionization region in the downstream. Calculations have also shown that the decrement of the stagnation pressure affects the plasma in nearly the same way as the increment of B. On the other hand, when both B and R_l are decreased as compared to the condition of Fig. 2, we get the result shown in Fig. 3e, in which small streamers generated at the channel entrance flow downstream and disappear repeatedly.

In the collision term A in energy Eq. (3), the δ value is usually chosen to be two. When we analyze the power generation experiments, real generator seems to have more loss of electron energy when compared to the theory. This causes difficulty in elevating the electron temperature. The reason for loss may be ascribed to the impurity and/or boundary flow effect on the plasma.[2] In order to account for the prevention of losses in elevating electron temperature, we assumed a large δ for our calculation. The results are shown in Fig. 3f, where the plasma of "state-1" flows repeatedly in the upstream region. This behavior of the plasma can also be obtained for low Joule heating conditions even if $\delta=2$.[18]

As shown above, the Joule heating condition introduces various types of plasma behavior inside the generator. The V-I characteristics which we have obtained for several load resistances are plotted in Fig. 4. In this figure, the results obtained from the steady-state local plasma analysis using the empirical relation for σ_{eff} and β_{eff} are shown by a solid curve.[13] The Hall current is kept almost constant for $R_l<1\Omega$ in our calculation, because the state-2 region becomes dominant as R_l decreases. The r-z analyses agree well with the empirical V-I characteristics in this region of load resistance. But the results of our analysis do not agree with the semi-empirical relation for large R_l, which correspnds to the condition of noble gas ionization. This suggests that the r-z dimensional analyses cannot simulate the behavior of the unstable plasma with noble gas ionization.

Discussion

The above results indicate that instability due to the partial ioniation of seed grows in two states, state-1 and state-2. This means that if the total Joule heating in the generator based on B and R_l is not enough to ionize all seed atoms in the channel, the plasma develops locally into two states, the fully ionized state and the slightly-ionized state. When this type of instability occurs, the volume ratio of these two states in the channel determines the generator performance.

The relations between the electron temperature in state-1 [T_e (1)] and the volume ratio γ of state-1 to the generator are shown in Fig. 5 for several values of magnetic field and load resistance. It is seen from the figure that in these gas conditions the increment of R_l raises γ, while the increment of B elevates T_e itself in state-1 region. Also shown in this figure are the contour lines of constant Joule heating in the whole generator. We find that increments of both B and R_l cause the higher total Joule heating; however, the magnetic field and load resistance lead in different effects on the generator. The density of the Joule heating in both states mainly depends on B, so that the electron temperature in each state is determined by B. On the other hand, the ratio γ is mainly determined by R_l because the generator must be electrically balanced with the load resistance.

In the instability regime the output current usually fluctuates. The fluctuation can be explained by the variation of γ and T_e (1) as mentioned earlier. In Fig. 6, the evolutionary feature of n_e distribution for the same condition as in Fig. 3b is exhibited. For these two cases, the initial distribution of perturbations of T_e, i.e., the series of random numbers giving the perturbation, is different. Comparing these two figures, we can see that the plasma for these two cases grows in different ways and the inlet relaxation in Fig. 6 is narrower than that in Fig. 3b. This means that the steady-state plasma cannot be

uniquely decided but changes with external small disturbance. In general, many perturbations are introduced to the generator because of the fluctuation of gasdynamic conditions. As a result, the plasma in the generator changes every moment, which produces the fluctuation of output power.

The fluctuation of the output current can also be explained by the steady-state analysis of the MHD equations. To simplify the problem, we assume the steady-state energy equation as

$$J^2/\sigma = A \tag{7}$$

and the Saha equilibrium condition. Including the Ohmic equations with Eq. (7), we can get the r-component of current density J_r as a function of T_e. The results are shown in Fig. 8, where two branches of J_r are found: J_r (1) which corresponds to generating current ($J_\theta < 0$) and J_r (2) which corresponds to consuming current ($J_\theta > 0$). The region where J_r is illustrated by bold line represents the fully-ionized seed region obtained from the linear instability analysis. It should be noticed that we could not exactly determine J_r, but it is expected to suffer from a fluctuation in the region shown with bold line. In other words, the instability does not have a definite steady state. When a J_r is given, the T_e of both states are determined by point A and B shown in Fig. 7. Here the state which corresponds to C could not appear to be in steady state because the state is locally unstable.[11] We can find that J_θ in state-2 directs oppositely to the J_θ in the state-1; hence, the state-2 plasma is stable. When T_e in each state is decided for a given J_r, the volume ratio γ is determined to give a generator and load resistance that match.

The variations of γ with T_e (1) for several load resistances are shown by solid line in Fig. 8. Here we will also show the results of r-z dimensional simulation. The hatched region illustrates the available region of the two-state plasma model. It is found that the simplified steady-state analysis is in good agreement with the time-dependent analysis. The contour lines of constant Joule heating in the whole generator channel are also drawn in this figure where it is seen that the total Joule heating must take some suitable values to realize the two-state plasma model. If the Joule heating becomes lower than that corresponding to the lower left corner of the hatched region, another type of instability occurs, which is shown in Fig. 3e. On the other hand, Joule heating compared to that corresponding to the upper right corner of the region produces instability due to partially ionized noble gas atoms, which is beyond the scope of our present discussion.

The r-θ analysis carried out near the fully ionized seed condition shows that the plasma in disk channels consists of the regions of inlet relaxation and fully ionized seed plasma, each of which is almost uniform and stable. The shape of the boundary between these two regions is almost a concentric circle.[4,5] Thus, the assumption $\partial/\partial\theta = 0$ is reasonably valid. This situation in the r-θ plane corresponds to the final state in Fig. 2 or Figs. 3a–3c.

When R_l is small, the r-θ analyses show several very sharp spiral streamers flowing with the fluid, and $\partial/\partial\theta = 0$ is not strictly valid.[6] Although the detailed structure and behavior of the streamers may not be obtained from the r-z analysis, both analyses lead to almost the same result regarding the macroscopic properties of plasma such as the Hall voltage, two-state nature of plasma, the volume ratio of each state, and T_e in state-1, as far as we restrict the question to the partial and full ionization of seed region.[17,18] However, the instability due to the partial ionization of noble gas atoms cannot be described by our two-state nature of plasma, or by the r-z simulation. This indicates that the spatial structure of instability due to the partial ionization of noble gas is different from that due to seed. This fact corresponds to the fact that the results of the r-z analysis and the semi-empirical relation are in good agreement regarding the V-I characteristics for R_l which gives the partial or full ionization of seed atoms

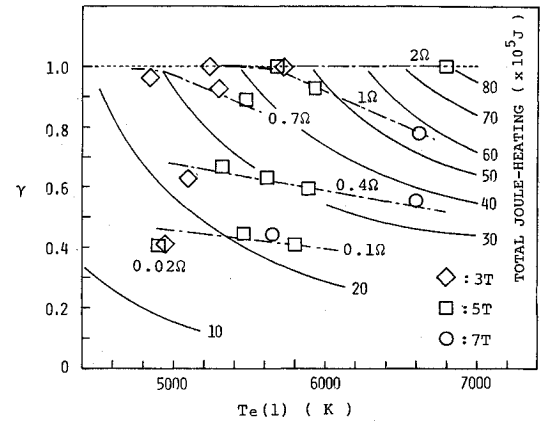

Fig. 5 Variation of γ, T_e in the state 1 and the total Joule heating in the channel with B and R_l.

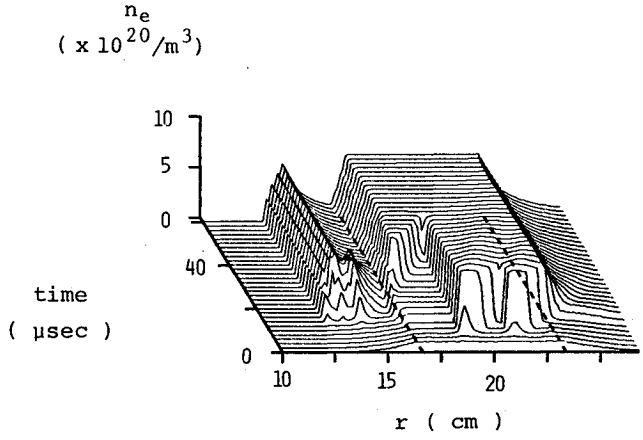

Fig. 6 Another evolution of the distribution of n_e in the r-direction for the channel.

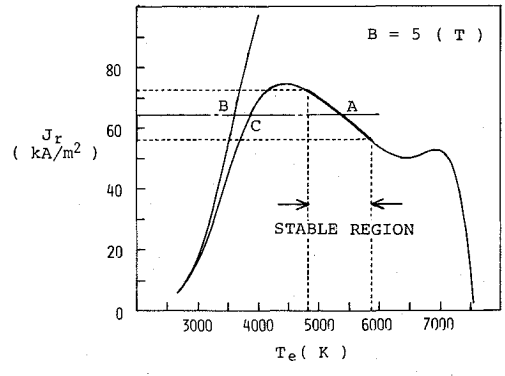

Fig. 7 Relation between J_r and T_e expressed by Eq. (7).

$R_l < 1\Omega$; however, they are not in agreement when R_l is larger than 1Ω.

Effect of Boundary Layer

Assumption for the Boundary Layer

It is an advantage in the r-z plane analysis that we can take account of the boundary layers. In this section, we show the results including the effect of the boundary layer. In the

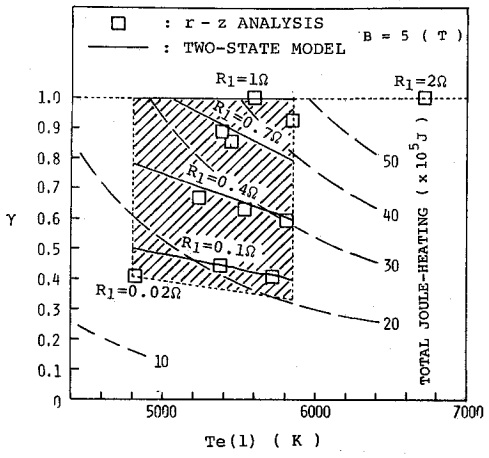

Fig. 8 Variation of γ and the total Joule heating in the channel with T_e in the state-1 and R_l by the simple two-state model.

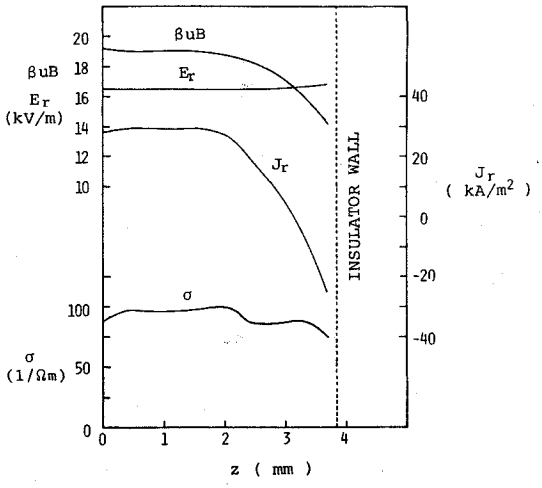

Fig. 10 Distribution of βuB, E_r, σ, and J_r along the z-direction.

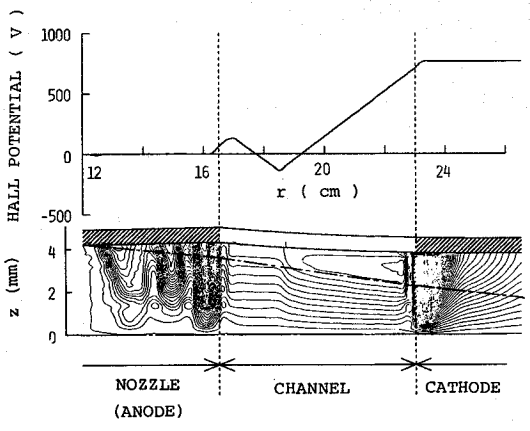

Fig. 9 Current stream line in the r-z plane and the distribution of Hall potential, $B=7T$, $R_l=4\Omega$. Total current of the generator I_t is 190 A. Bold chain line shows the region of boundary layer flow.

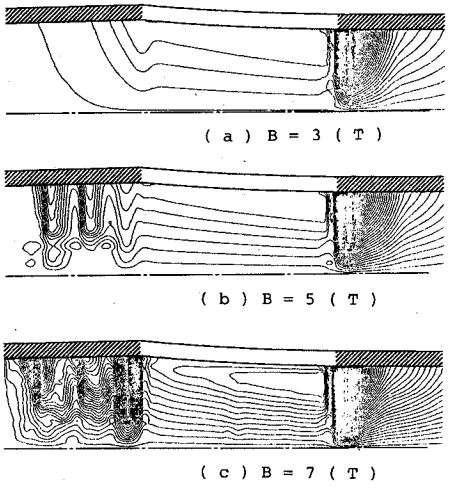

Fig. 11 Effect of the magnetic field on the current streamline in steady-state, $R_l=6\Omega$.

calculations, we assume that the boundary layer thickness is proportional to the distance from the nozzle throat, and that the one-seventh power law is adopted for the gas velocity and temperature. The displacement thickness is taken as one-half of the boundary layer thickness, and the channel height is extended by adding the displacement thickness to the height of the constant cross-section channel. The profile of boundary layer is shown in Fig. 9 together with simulation results. Here we can again assume the constant gas velocity and temperature in the mainflow, as in the case of constant cross-section channel.

Eddy Current in the Boundary Layer

Figure 9 shows a typical example of current pattern in the r-z plane and the distribution of electrical potential along the r-direction. The scale used in the z-direction is more magnified than that in the r-direction. In this example, the plasma inside the channel consists of the state-1 and state-2, which occupy the downstream and the upstream region, respectively, as it can be seen from th shape of the potential distribution curves. In the state-2 plasma, the eddy current arises in the boundary layer. The eddy current shares about 20% of the total amount of current that is 190 A. On the other hand, the eddy current does not occur in the state-2 plasma.

Figure 10 shows the distributions of the electrical conductivity σ, the electromotive force βuB, E_r, and J_r along the z-direction at $r=22$ cm. It can be seen that σ and E_r hardly change along the z-direction while βuB becomes small in the boundary layer because it decreases proportionally with the fluid velocity. The eddy current in the boundary layer occurs when βuB becomes less than E_r. In general, the large σ in the boundary layer promotes this eddy current.

In subsonic open-cycle MHD generators, σ becomes small in the thermal boundary layer because it is determined mainly by the gas temperature, and the eddy current in the boundary layer on the insulator walls hardly arises.[14,15] On the other hand, in the closed-cycle MHD generator, σ hardly reduces in the boundary layer as shown in Fig. 10 because of the non-equilibrium effect. Thus, the eddy current is considered to be larger in closed-cycle MHD generators than in those with open cycles.

Current Distribution in Nozzle

Figure 9 also shows that plasma properties are inhomogeneous in the nozzle (anode) and in the cathode region. Figure 11 shows the current streamline in the generator for several magnetic fields. For small B, T_e and n_e in the nozzle are uniform and low, and the current cannot enter the nozzle region. On the other hand, when B is large, several enhanced eddy currents arise in this region. This can also be seen from Figs. 3a–3e, which show that the plasma properties in the nozzle do not depend on R_l. The very intensive eddy current appears at the upperstream edge of the cathode in all cases of Fig. 11.

Figure 12 shows the temporal development of the current pattern for the case of strong magnetic field. Small perturbations added initially to T_e and n_e make spots where σ is slightly

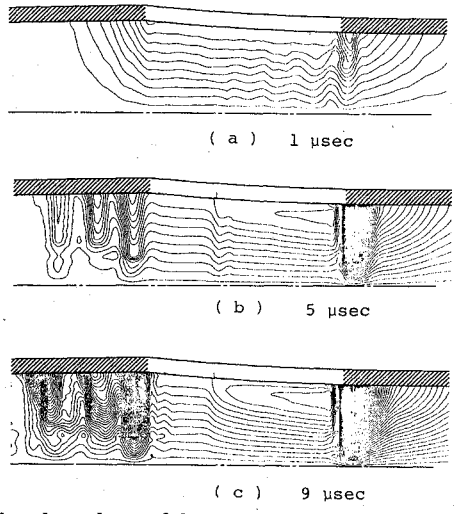

Fig. 12 Time dependence of the current streamlines, $B=7T$, $R_l=4\Omega$.

larger than that in surrounding. In the nozzle, the eddy current arises between these spots and the anode due to the shortage of induced Hall field on the electrode surface, since the electrical conductivity in the z-direction is much higher than those in the r- and θ-directions. This eddy current elevates T_e and n_e in this region and grows turbulently. The electron density n_e in the cathode region is kept rather large because the fully ionized seed plasma in the channel flows onto this region, whereas T_e decreases more rapidly there than n_e. Thus σ becomes especially large in the cathode region, which enhances the eddy current.

In the case of small B, n_e is so small in the nozzle that the condition of electron collision may not play a dominant role, i.e., the Boltzmann distribution of electron velocity may not hold.[12] This effect is supposed to result in a remote possibility of plasma ignition. On the other hand, when B is sufficient, the current in the nozzle can cause the pre-ionization effect as stated in the previous section. An example of pre-ionization effect has been shown in Fig. 6, where the large n_e produced by the disturbed current in the nozzle flows toward the inlet of the generator and leads to the disappearance of the relaxation region.[19]

Conclusion

From our analysis of the time-dependent MHD equations for the nonequilibrium plasma in the r-z plane, the following conclusions can be drawn.

1) The instability of MHD plasma, due to the partial ionization of seed atoms, grows along the flow direction and converges to two states, one a weakly ionized seed state and the other a fully ionized seed state. The weakly ionized seed state causes the reduction of the generator performance. Parameters, such as magnetic field and stagnation pressure, control the plasma characteristics in each state, while external load resistance mainly determines the volume ratio of the two states in the channel. The stable, fully ionized seed plasma can be established in almost the whole channel by choosing suitable plasma parameters. 2) In the case of small external load resistance, the streamer formed in the inlet region of the channel flows downstream, and the large relaxation region appears in the inlet region of the channel. 3) The eddy current occurs in the boundary layer when the Hall field is high. 4) When the magnetic field is large, several eddy currents appear in the nozzle, and this current causes pre-ionization effect. Also, the very intensive eddy current arises at the upstream edge of the cathode.

Acknowledgment

The authors are grateful to Profs. S. Shioda and Prof. H. Yamasaki, and Mssrs. N. Harada, Y. Yoshikawa and Y. Okuno for constant encouragement and their useful discussions throughout this work. The authors also wish to thank Mr. D. Biswas for valuable suggestions and English improvement. Part of this work is performed as cooperative research with Plasma Laboratory of Nagoya University and is supported by the grant-in-aid for energy research from the Ministry of Education.

References

[1]Sens, A.F.C., Veefkind A., Uhlenbusch, J.F., and Rietjens, L.H.Th., "Experimental Studies on a Closed Cycle MHD Disk Generator," *8th International Conference on MHD,* Vol. 4, 1983, pp. 164–172.

[2]Yamasaki, H., et al., "Recent Results of Power Generation Experiments with the Fuji-1 Facility," *Proceedings of the 22nd Symposium of Engineering Aspects of MHD,* 1984 p. 3.4.1.

[3]Harada, N., Yamasaki, H., Oyake, T., Matsusaki, A., Shimizu, S., Hiratsuka, K., and Shioda, S., "Effect of Stagnation Gas Pressure and Magnetic Field Strength on Fully Ionized Seed Closed Cycle MHD Generators," *8th International Conference on MHD,* Vol. 4, 1983, pp. 181–184.

[4]Yoshikawa, Y., Kabashima, S., Yamasaki, H., Harada, N., and Shioda, S., "Dynamical Behavior of Disk Type Closed Cycle MHD Generator II," *Proceedings of the 22nd Symposium of Engineering Aspects of MHD,* 1984, p.3.2.1.

[5]Yoshikawa, Y., Kabashima, S., Harada, N., and Shioda, S., "Dynamical Properties of Nonequilibrium Plasma in Disk MHD Generator," *Journal of Propulsion and Power,* Vol. 1, Nov.-Dec. 1985, pp. 425–431.

[6]Inui, Y., Hara, T., and Umoto, J., "Numerical Simulation of the Discharge Structure in Nonequilibirum Disk Type MHD Generator," *Proceedings of 23rd Symposium on Engineering Aspects of MHD,* 1985, pp. 461–475.

[7]Rosa, R.J., "Magnetohydrodynamic Energy Conversion," McGraw-Hill Book Company, New York, 1963, Chapter 4.

[8]Mitchner, M. and Kruger, C.H., "Partially Ionized Gases," John Wiley & Sons, New York, 1973, Chap. 4.

[9]Teare, J.D., Loubsky, W.J., Lytle, J.K., and Louis, J.F., "Optimization of Disk Generator Performance for Base-Load Plant Systems Application," *Proceedings of 7th International Conference on MHD,* Vol. 2, 1980, pp. 644–652.

[10]Mesland, A.J., "Nonlinear Behavior of the Electrothermal Instability in Nonequilibrium MHD Plasma," *Eighth International Conference on MHD,* Vol. 4, 1983, pp. 130–135.

[11]Hara, T., Umoto, J., and Inui, Y., "Numerical Analysis of the Nature of the Streamers in Noble Gas MHD Generators," *Eighth International Conference on MHD,* Vol. 4, 1983, pp. 136–139

[12]Kerrebrok, J.L., "Nonequilbirium Ionization Due to Electron Heating: I. Theory," *AIAA Journal,* Vol. 2 1964, pp. 1072–1080.

[13]Solbes, A., Nakamura, T, and Kerrebrock, J.L., "Electrothermal Instability in Plasmas with Current Flow Parallel to the Magnetic Field," *Proceedings of 11th Symposium of Engineering Aspects of MHD,* 1970, pp 209–215.

[14]Roseman, D., Nakamura, T., and Eustis, R.H., "Current Distribution and Nonuniformities in MHD Disk Generators," *Proceedings of the 19th Symposium of Engineering Aspects of MHD,* 1981, pp. 3.2.1.

[15]Nakamura, T., "An Integral Method Analysis of the Disk Generator Boundary Layer," *Proceedings of the 20th Symposium of Engineering Aspects of MHD,* 1982, pp. 6.6.1.

[16]Hiramoto, T., "Rates of Total and Local Radiative Energy Losses in Nonequilibrium Plasma, *Journal of the Physical Society of Japan,* Vol. 26, 1969, pp. 785–801.

[17]Kabashima, S., Yoshikawa, Y., Okuno, Y., Shimizu, E., Yamasaki, H., and Shioda, S., "Instability and Fluctuation of Output Voltage of Disk Type Closed Cycle MHD Generator," *Proceedings of the 23rd Symposium on Engineering Aspects of MHD,* 1985, pp. 624–635.

[18]Kabashima, S., Matsubara, H., Okuno, Y., and Yoshikawa, Y., "Fluctauation of Output Power and Instability of Plasma in Closed Cycle MHD Power Generation," *U.S./Japan Seminar on MHD Power Generation,* March 1986, pp. F1–F15.

[19]Harada, N., Yamasaki, H., and Shioda, S., "Experiments in Shock-Tube Driven Closed Cycle MHD Generator with Seeded Helium," *U.S./Japan Seminar on MHD Power Generation,* March 1986, B15–B27.